PHYSICAL REVIEW E VOLUME 48, NUMBER 6 DECEMBER 1993

Chaotic Turing-Hopf mixed mode

A. De Wit, G. Dewel, and P. Borckmans
Service de Chimie Physique and Centre for Nonlinear Phenomena and Complex Systems, Université Libre de Bruxelles, Case Postale 231, 1050 Brussels, Belgium
(Received 6 July 1993)

An alternative scenario for the onset of spatiotemporal chaos in one-dimensional extended systems arising from a phase instability of a Turing-Hopf mixed mode is presented. This mechanism leads to weak and defect turbulences. The transition between these two is either continuous or hysteretic, depending on the values of the parameters.

PACS number(s): 47.20.−k, 05.45.+b

The study of spatiotemporal chaos in driven extended systems has been the focus of a large activity these last years [1]. One scenario has been clearly identified where the Benjamin-Feir instability of a homogeneous limit cycle first drives the system into a regime of weak turbulence [2] followed by a more chaotic state characterized by the proliferation of topological defects (*defect turbulence*) [3,4]. On the other hand, the homogeneous steady states of reaction-diffusion systems may also be destabilized by another type of diffusion-driven instability leading to Turing patterns [5]. These steady periodic concentration structures have now been obtained experimentally in open gel reactors [6,7]. In the region where Turing and Hopf bifurcations interact, spatiotemporal complexity may appear in these experimental patterns [8,9]. The scenario presented above can, however, not explain this "chemical turbulence," as the Benjamin-Feir and the Turing instabilities are mutually exclusive for most reaction-diffusion systems [2,10]. In this Rapid Communication we report an alternative mechanism based on the phase instability of mixed Turing-Hopf modes which may arise in the vicinity of the Turing-Hopf codimension-2 point [11,12]. We focus here on one dimensional (1D) systems.

In the vicinity of this codimension-2 point the concentration field $\mathbf{c}$, which appears in the chosen reaction-diffusion system, may be expressed in terms of two complex amplitudes T and H:

$$\mathbf{c}(x,t) = \mathbf{c}_0 + \mathbf{e}_T T e^{iq_c x} + \mathbf{e}_H H e^{i\omega_c t} + \text{c.c.} \tag{1}$$

$\mathbf{c}_0$ is the uniform reference state, $\mathbf{e}_T$ and $\mathbf{e}_H$ are respectively the critical Turing and Hopf eigenvectors of the linearized reaction-diffusion operator. ω_c is the critical frequency of the limit cycle while q_c is the critical Turing wave vector. c.c. stands for complex conjugate. The competition between these modes can be described by amplitude equations that are obtained by the use of standard techniques of bifurcation analysis [13]. If X and τ are the slow space and time scales, then [11]

$$\frac{\partial T}{\partial \tau} = \mu_T T - g|T|^2 T - \lambda |H|^2 T + D^T \frac{\partial^2 T}{\partial X^2}, \tag{2}$$

$$\frac{\partial H}{\partial \tau} = \mu_H H - (\beta_r + i\beta_i)|H|^2 H - (\delta_r + i\delta_i)|T|^2 H + (D_r^H + iD_i^H)\frac{\partial^2 H}{\partial X^2}, \tag{3}$$

where μ_H and $\mu_T = \mu_H + \nu$ are the two unfolding parameters. We assume in the following that g, β_r, D^T, and D_r^H are positive so that both bifurcations are supercritical.

The dynamical system of Eqs. (2) and (3) possesses three nontrivial global solutions:

(i) a family of Turing structures,

$$T = \left\{ \frac{\mu_T - D^T Q^2}{g} \right\}^{1/2} e^{iQX}, \quad H = 0; \tag{4}$$

(ii) a one-parameter family of plane waves,

$$T = 0, \quad H = \left\{ \frac{\mu_H - D_r^H K^2}{\beta_r} \right\}^{1/2} e^{i(\Omega_K \tau - KX)} \tag{5}$$

with the frequency renormalization, $\Omega_K = -\beta_i |H_K|^2 - D_i^H K^2$, where H_K is the preexponential factor in H;

(iii) a two-parameter family of mixed modes,

$$T = \left\{ \frac{\beta_r(\mu_T - D^T Q^2) - \lambda(\mu_H - D_r^H K^2)}{\Delta} \right\}^{1/2} e^{iQX},$$

$$H = \left\{ \frac{g(\mu_H - D_r^H K^2) - \delta_r(\mu_T - D^T Q^2)}{\Delta} \right\}^{1/2} \times e^{i(\Omega_{KQ}\tau - KX)} \tag{6}$$

with $\Delta = \beta_r g - \lambda \delta_r$ and $\Omega_{KQ} = -\beta_i |H_{KQ}|^2 - \delta_i |T_{KQ}|^2 - D_i^H K^2$, where H_{KQ} and T_{KQ} are the preexponential factors of H and T. The relative stability of these three sets of modes may lead to various bifurcation scenarios. When $\Delta < 0$, the mixed mode is always unstable and bistability between the limit cycle and the Turing mode occurs. Various localized structures have been characterized in this domain [14]. In the following, we concentrate on situations where the mixed modes are stable toward spatially homogeneous perturbations ($\Delta > 0$). This condition can indeed be fulfilled for some range of

parameters in reaction-diffusion systems. On increasing the bifurcation parameter μ_H one then typically observes the following sequence of states (when $\nu > 0$): Turing structures $\rightarrow$ mixed mode $\rightarrow$ homogeneous oscillations. In the absence of spatial modulations, Eqs. (2) and (3) are invariant under the transformations $T \rightarrow Te^{i\theta}$ and $H \rightarrow He^{i\phi}$. As a result, the corresponding linearized matrix about the mixed state has two zero eigenvalues. When spatially inhomogeneous perturbations are taken into account these marginal modes may induce diffusive instabilities of the phases. In particular, the most stable mixed mode ($Q = 0, K = 0$) undergoes such an instability when

$$\mathcal{D} = \frac{D_i^H(\beta_i g - \lambda\delta_i) + D_r^H(\beta_r g - \lambda\delta_r)}{\Delta} < 0. \qquad (7)$$

Let us remark that the standard Benjamin-Feir instability criterion of a homogeneous limit cycle is recovered when all the parameters related to the coupling between the two modes are set equal to zero, i.e.,

$$D_i^H\beta_i + D_r^H\beta_r < 0. \qquad (8)$$

It is important to note that the inequality (7) may be satisfied even when (8) is not fulfilled, i.e., when the limit cycle is stable with respect to the modulational instability.

We have numerically integrated Eqs. (2) and (3) by means of a fourth-order Runge-Kutta scheme (NAG library) complemented by finite-difference methods. The behavior of the system is followed on a system of length $L = 512$ with periodic boundary conditions. These simulations show that, when $\mathcal{D} < 0$, the mixed mode is indeed unstable. According to the value of the parameters, the system enters then either a phase-turbulent regime similar to that of the Kuramoto-Sivashinsky equation [15,16] or a defect chaos regime [2,17] characterized by phase defects and large-amplitude fluctuations on both T and H.

These dynamics can be illustrated by space-time maps of the concentration $\mathbf{c}(x,t)$ and of the amplitude and phase of the Hopf mode (Fig. 1). In the example shown here, the parameters are chosen such that an initially stable mixed mode is brought into a defect chaos regime after one-third of the time run. In the first part of the time, we see that the lines of constant phases are continuous [Fig. 1(a)]. The amplitudes of the Turing and Hopf modes are constant [Fig. 1(b)]. The concentra-

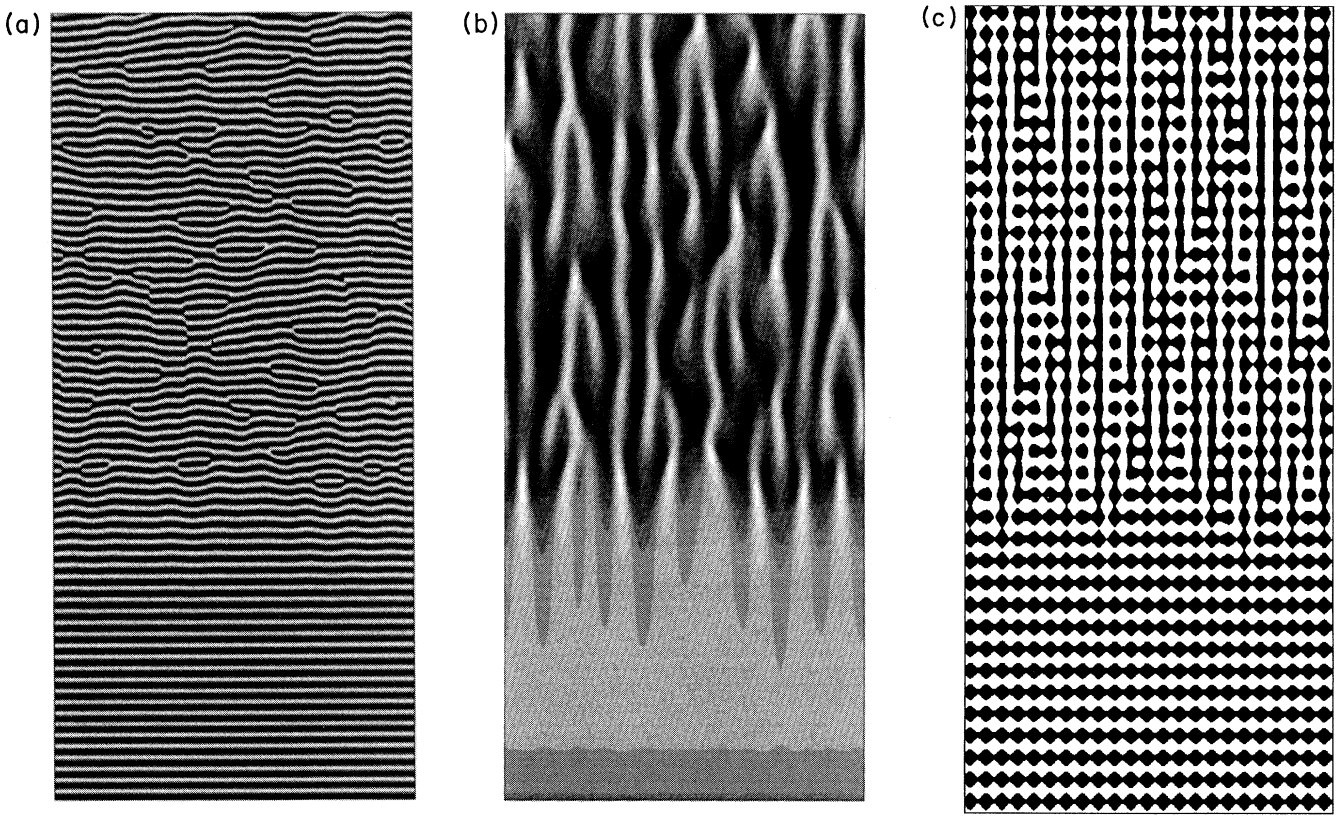

FIG. 1. Space-time plots representing the evolution in a 1D box of length 512 during 700 units of time (running upwards). We bring a stable mixed mode in the region of instability toward defect chaos. The parameters are $\mu_H = 0.3, \mu_T = 0.5, g = 2, \lambda = 1.5, \beta_r = \delta_r = D_T = D_r^H = 1$. We take $D_i^H = 5, \beta_i = 1.6, \delta_i = 3$. Highest values are in white. (a) Lines of constant phase of the Hopf mode. Spatiotemporal defects of phase appear at the points where the amplitude of the Hopf mode locally reaches zero. (b) Amplitude of the Hopf mode. (c) Concentration $\mathbf{c}$ reconstructed as $Te^{i0.28x} + He^{i0.33t}$ + c.c. We recognize in the first third of time the "polygonal" space-time pattern characteristic of a mixed mode.

tion **c** is periodic both in space and time leading to a "polygonal" space-time pattern characteristic of a mixed mode [Fig. 1(c)]. In the second part of the time, the defect chaos regime exhibits on the contrary space-time phase dislocations appearing when the amplitude of the Hopf mode locally reaches zero. On the other hand, in the phase chaos regime the amplitudes of the Turing and Hopf modes are fluctuating around their stationary value because the phase of the Hopf solution is turbulent. This weak type of chaos cannot be clearly distinguished on space-time plots from the stable mixed mode, because, though the phase fluctuates, lines of constant phase remain continuous. This phase chaos dynamics is therefore not represented in the figure.

We have studied the transition between the two forms of turbulence by plotting the absolute minimum of the amplitude of the Hopf mode $H_{\min}$ in a given space-time area versus β_i or δ_i. This method clearly distinguishes between transitions of first and second order. In this latter case, the transition between phase and defect chaos is continuous like in the conditions of Fig. 2(a). On the contrary, for first-order transitions there is a hysteresis phenomenon characteristic of bistability between phase and defect chaos [Fig. 2(b)]. We use these graphs to determine the transition points between both regimes. The behavior of the system is then considered for different sets of parameters. In the (δ_i, β_i) plane, the transition between phase and defect chaos appears to be always discontinuous, leading to a hysteretic behavior, as summarized in Fig. 3(a). On the contrary, in the (D_i^H, β_i) plane, both first- and second-order transitions can be observed [Fig. 3(b)]. Moreover, the defect chaos regime may persist in the stable region of this plane where it

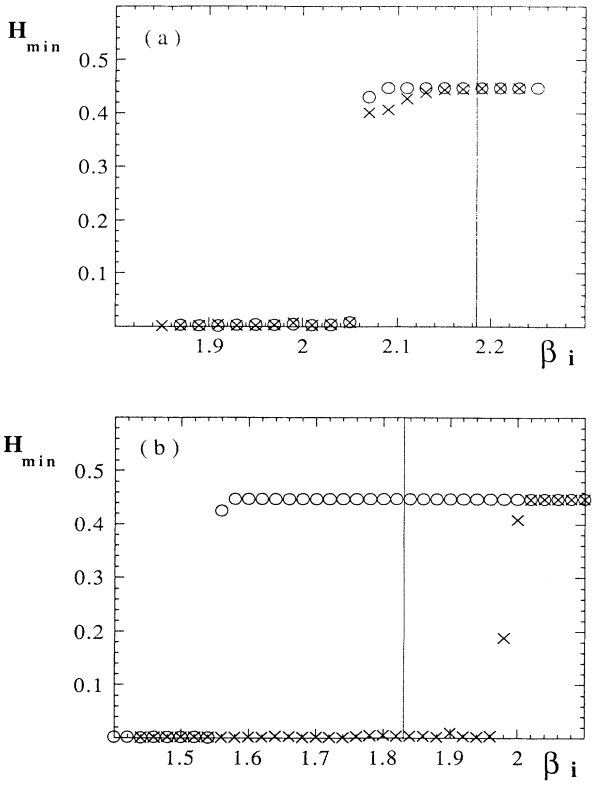

FIG. 2. Minimum of the amplitude of the Hopf mode $H_{\min}$ vs parameter β_i. Following a delay of 3000 units of time after a quasistatic increase (crosses) or decrease (circles) of β_i, $H_{\min}$ is determined in a space-time area of 512 × 500. The solid line stands for the stability limit of the mixed mode [Eq. (7)]. (a) $D_i^H = 4$. Continuous bifurcation characteristic of a second-order transition; (b) $D_i^H = 0.6$. Hysteresis typical of a first-order transition. Below the stability limit of the mixed mode ($\beta_i = 1.83$), defect chaos coexists with the phase chaos regime. For $\beta_i > 1.83$, defect chaos coexists with the stable mixed mode. Note that the measure of $H_{\min}$ is not a good means to distinguish a stable mixed mode from phase chaos of the mixed mode. All other parameters are the same as in Fig. 1.

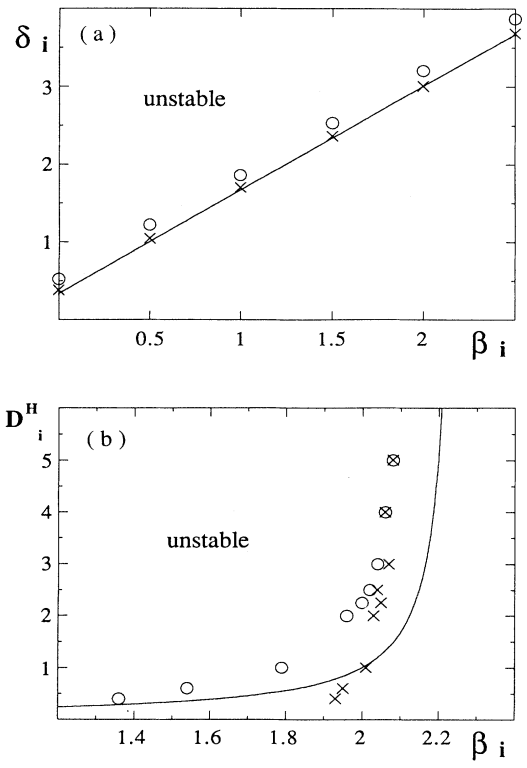

FIG. 3. Phase planes (δ_i, β_i) and (D_i^H, β_i) summarizing the region of stability of the phase and defect chaos. The solid line corresponds to the limit of stability of the Turing-Hopf mixed mode [Eq. (7)]. (a) (δ_i, β_i) plane for $D_i^H = 1$. Crosses stand for the lower limit of stability of the defect chaos regime when δ_i is decreased, while circles represent the upper limit of stability of the phase chaos dynamics when δ_i is increased. The transition between phase and defect chaos regimes is hysteretic (bichaos). (b) (D_i^H, β_i) plane for $\delta_i = 3$. Crosses stand for the upper limit of stability of the defect chaos regime when β_i is increased, while circles represent the lower limit of stability of the phase chaos dynamics when β_i is decreased. Transitions of second order between the two regimes are observed for higher D_i^H's. For lower D_i^H's, the transition is of first order (bichaos). Moreover, defect chaos may persist in the region where the mixed mode is stable. All other parameters are the same as in Fig. 1.

thus coexists with the stable mixed mode [Figs. 2(b) and 3(b)].

We have shown that the mixed modes resulting from the interaction between Turing and Hopf modes may become unstable toward diffusion-induced phase instabilities. This bifurcation gives rise to weak and strong spatiotemporal chaos in the sense that two different regimes of phase and defect chaos are observed. This behavior is reminiscent of the dynamics of the one-dimensional complex Ginzburg-Landau equation beyond the Benjamin-Feir instability [4]. Its origin lies however genuinely in the coupling between Turing and Hopf modes. Indeed, for the values of parameters we have chosen, the complex Ginzburg-Landau equation alone [i.e., Eq. (3) with $\delta_r = \delta_i = 0$] does not exhibit a Benjamin-Feir instability. However, when it is coupled with the amplitude equation for the Turing pattern, the corresponding mixed mode may undergo a phase instability as shown here. From a theoretical point of view, one may test these two phase instabilities to determine if the characteristics of chaotic behaviors may be described in terms of similar universal laws and properties. Moreover, this new mechanism offers another scenario for the onset of spatiotemporal chaos in all degenerate systems where two instabilities breaking, respectively, spatial and temporal symmetry interact. Experimentally, this may be relevant to recent experimental observations in gas discharge [18] and chemical [9] systems. In the latter case, the Turing patterns obtained in the chlorite-iodide–malonic acid (CIMA) reaction arise because the activator species forms a complex of low mobility with starch, the color indicator of the reaction [19]. This gives rise to the difference between the effective mobilities of the reactants necessary to shift a competing Hopf bifurcation so that the Turing structures may exist. When this complex formation effect is progressively relaxed, the shift fades away and both bifurcations start interacting. It is in this transition region that the complex spatiotemporal behaviors have been observed. In this regard, the study of spatiotemporal chaos in a chemical reaction-diffusion model has also been undertaken.

We thank P. Coullet, P. De Kepper, P. Gaspard, G. Nicolis, and A. Pumir for stimulating discussions. P.B. and G.D. received support from the FNRS (Belgium) and A.D. received support from IRSIA (Belgium). This work was supported by the EC Science Program (Twinning No. SC1-CT91-0760).

[1] See *Nonlinear Evolution of Spatio-Temporal Structures in Dissipative Continuous Systems*, edited by F. Busse and L. Kramer (Plenum, New York, 1992).
[2] Y. Kuramoto, *Chemical Oscillations, Waves and Turbulence* (Springer, Tokyo, 1984).
[3] P. Coullet, L. Gil, and J. Lega, Phys. Rev. Lett. **62**, 1619 (1989).
[4] B.I. Shraiman, A. Pumir, W. van Saarloos, P.C. Hohenberg, H. Chaté, and M. Holen, Physica D **57**, 241 (1992).
[5] A. Turing, Philos. Trans. R. Soc. London Ser. B **237**, 37 (1952).
[6] V. Castets, E. Dulos, J. Boissonade, and P. De Kepper, Phys. Rev. Lett. **64**, 2953 (1990).
[7] Q. Ouyang and H.L. Swinney, Nature **352**, 610 (1991).
[8] Q. Ouyang and H.L. Swinney, Chaos **1**, 411 (1991).
[9] J.-J. Perraud, K. Agladze, E. Dulos, and P. De Kepper, Physica A **188**, 1 (1992).
[10] Y.X. Li, Phys. Lett. A **147**, 204 (1990).
[11] H. Kidachi, Progr. Theor. Phys. **63**, 1152 (1980).
[12] J.P. Keener, Stud. Appl. Math. **55**, 187 (1976).
[13] J. Guckenheimer and P. Holmes, *Nonlinear Oscillations, Dynamical Systems and Bifurcations of Vector Fields* (Springer-Verlag, Berlin, 1983).
[14] J.-J. Perraud, A. De Wit, E. Dulos, P. De Kepper, G. Dewel, and P. Borckmans, Phys. Rev. Lett. **71**, 1272 (1993).
[15] Y. Kuramoto, Suppl. Progr. Theor. Phys. **64**, 346 (1978).
[16] G.I. Sivashinsky, Acta Astron. **6**, 569 (1979).
[17] H. Sakaguchi, Progr. Theor. Phys. **84**, 792 (1990).
[18] H. Willebrand, F.-J. Niedernostheide, R. Dohmen, and H.-G. Purwins, in *Oscillations and Morphogenesis*, edited by L. Rensing (Dekker, New York, 1993), p. 81.
[19] I. Lengyel and I.R. Epstein, Proc. Natl. Acad. Sci. USA **89**, 3977 (1992).

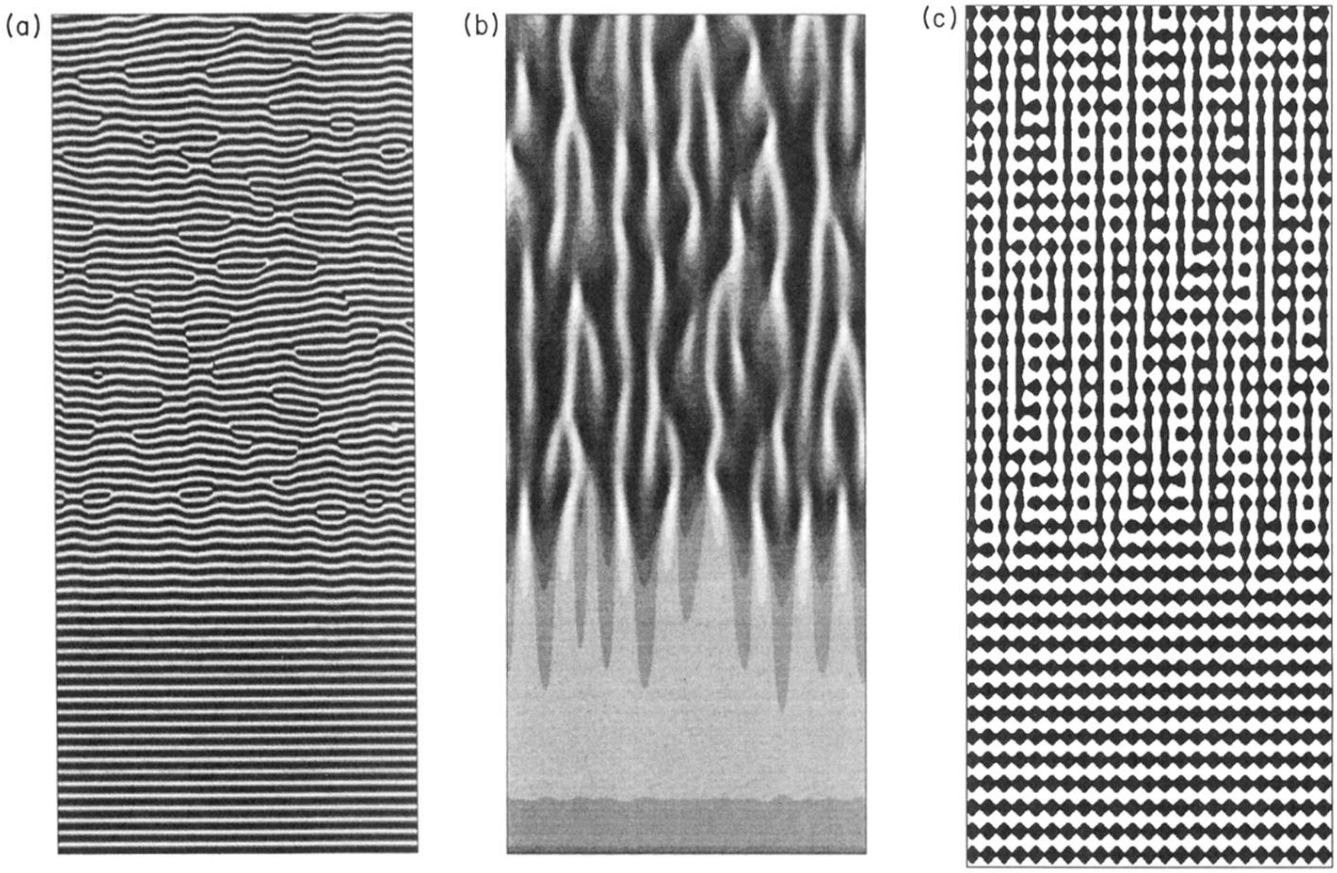

FIG. 1. Space-time plots representing the evolution in a 1D box of length 512 during 700 units of time (running upwards). We bring a stable mixed mode in the region of instability toward defect chaos. The parameters are $\mu_H = 0.3, \mu_T = 0.5, g = 2, \lambda = 1.5, \beta_r = \delta_r = D_T = D_r^H = 1$. We take $D_i^H = 5, \beta_i = 1.6, \delta_i = 3$. Highest values are in white. (a) Lines of constant phase of the Hopf mode. Spatiotemporal defects of phase appear at the points where the amplitude of the Hopf mode locally reaches zero. (b) Amplitude of the Hopf mode. (c) Concentration **c** reconstructed as $Te^{i0.28x} + He^{i0.33t}$ + c.c. We recognize in the first third of time the "polygonal" space-time pattern characteristic of a mixed mode.